ACS OMEGA

Open Access

http://pubs.acs.org/journal/acsodf

Article

Numerical Simulation of Component Transfer and Oil Drive of Nonalkali Ternary Emulsion Systems

Xiaoying Liu, Jingchun Wu,* Jingang He, Yinglong Xuan, Hao Wu, Sian Chen, Yuan Yuan, Haixiang Zhang, and Zhao Yang

Cite This: *ACS Omega* 2023, 8, 40051−40062

Read Online

ACCESS | Metrics & More | Article Recommendations

ABSTRACT: So far, alkali/surfactant/polymer flooding is widely used in oilfields to improve recovery. However, the introduction of alkali to the ternary composite leads to substantial damage formation, accelerates the scaling and corrosion loss in all aspects of surface injection and recovery, and consequently increases the cost of oil recovery in the ternary composite drive field. Therefore, environmentally friendly means are in urgent demand. Alternatively, a new non-alkali ternary drive system with salt instead of alkali has been developed based on the basis of ternary composite drive in the Daqing oilfield. In this experiment, a mathematical model of oil repelling by a salt-substituted alkali-free ternary emulsion system is formed, followed by the verification of the wet-lab experiments. The results show that the alkali-free ternary emulsion system can have a synergistic effect of complex salt and petroleum sulfonate surfactant and represents a wide range of ultralow interfacial tensions and good oil-repelling performances. The chromatographic separation occurs in the transmission process due to the adsorption of porous media, and the lower the permeability and the lower the injection rate, the higher the chromatographic separation degree. The use of multistage plug injection can narrow the difference of flow rate between high and low permeability layers and improve the recovery rate to 61.59%. Herein, the results provide theoretical guidance for the application of an alkali-free ternary emulsification system.

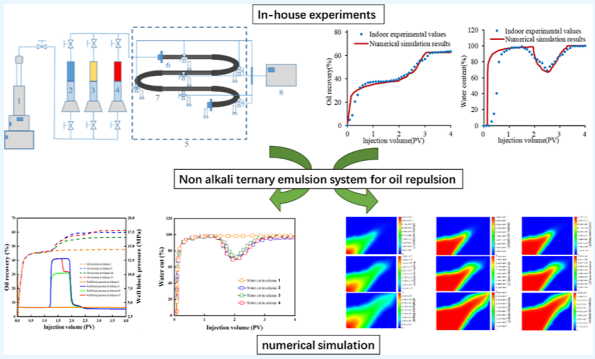

1. INTRODUCTION

The ternary composite, proposed in the 1980s, is an efficient drive oil technology, which has achieved rapid progress based on numerous indoor experimental studies and pilot mine experiments.[1−3] It is demonstrated that when the oil−water equilibrium interfacial tension reached an ultralow of 10^{-3} mN/m, crude oil recovery can be increased by more than 25% compared to the water drive recovery.[4] Ternary composite drives incorporate alkalis and surfactants compared with polymer drives. It can adsorb on the rock surface while increasing the wave volume and flush the crude oil out of the pore space by changing the wettability of the rock and the ultralow two-phase interfacial tension.[5−7] In summary, the ternary composite drive relies on two main means: one is to increase the system viscosity and the other is to reduce the oil−water interfacial tension.

The viscosity of the system relies mainly on polymers and varies depending on the oil formation conditions and injection parameters with the choice of different molecular weight products. The ultralow interfacial tension usually relies on the synergistic effect of alkali and surface activator. Herein, the surfactant plays the key role, while the type and addition of alkali is to improve the ultralow interfacial tension range and stability of the surface activator.[8−10] The addition of alkali substantially increases the formation damage and also accelerates the scaling and corrosion loss in all aspects of surface injection and recovery, which greatly increases the cost of oil recovery in the ternary composite drive mine. Hence, an alkali-free ternary emulsification system with efficient oil drive effect, low cost of chemicals, and light scaling has urgent demand. The composition of the alkali-free ternary emulsification composite system is different from the traditional ones, compounded by the unclear repulsion performance and chemical agent transport mechanism in the process. Therefore, the core repulsion experiment of the alkali-free ternary emulsification composite system is carried out to clarify the repulsion effect of the alkali-free ternary emulsification composite system on the remaining oil and the characteristics of each agent's transport principles.

Received: March 3, 2023
Accepted: September 28, 2023
Published: October 16, 2023

The chromatographic separation of the alkali-free ternary composite system will destroy the integrity of the ternary composite drive system, thus reducing the synergistic effect between salt and surfactant and deteriorating the oil displacement efficiency.[11] At present, it is believed that the long sand-filled tube model can better reflect the transport of each agent in different repellent stages by means of subnode sampling, which is the main means to analyze and study the chromatographic separation of composite drive indoor experiments. Li et al. conducted flow setup of a ternary composite oil repellent system in a sand-filled tube model and investigated the effects of wettability, permeability, and percolation distance on chromatographic separation of the ternary composite oil repellent system.[12] The same experiment is set on artificial homogeneous core by Corredor, and the effects of injection volume, viscosity, and injection method on oil-repellent effect and chromatographic separation were studied.13−15 Liu et al. analyzed the effects of injection rate and core permeability on chromatographic separation at the entrance end of cores on oil-free homogeneous cores.[16] In the alkali-free ternary composite system, the component salt itself has a passivating effect with the metal surface. Reducing the amount of alkali in the ternary composite system can effectively slow the occurrence of corrosion and scaling, making it easier for the ions ionized by the surfactant after dissolving in water to adhere to the rock surface. It can form a greater repulsive force while having the same charge to flow with water to ensure smooth replacement of crude oil and improve the recovery rate. Herein, we established the equation for the change of physical properties in porous media at the component transport equation level of the alkali-free ternary emulsion composite system, solved the mathematical equations discretely by using the finite difference method, and validated the numerical simulation results and indoor physical simulation experiments.

2. RESULTS AND DISCUSSION

2.1. Model Validation Results. Figures 1 and 2 show the dynamic change curves of recovery rate and water content,

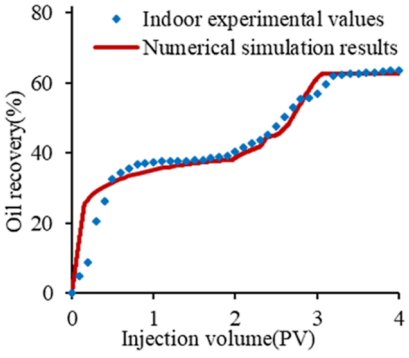

Figure 1. Variation in experimental versus numerical model recovery.

respectively. Comparing the results of indoor experiments and numerical simulations, it can be seen that the numerical simulation results are closer to the experimental values, the recovery degree of water drive simulation stage is 38.52%, the experimental value is 39.28%, the error rate is 1.97%, the recovery degree of alkali-free ternary emulsification compound drive simulation stage is 24.04%, the experimental value is 24.41%, and the error rate is 1.54%. The total recovery of the

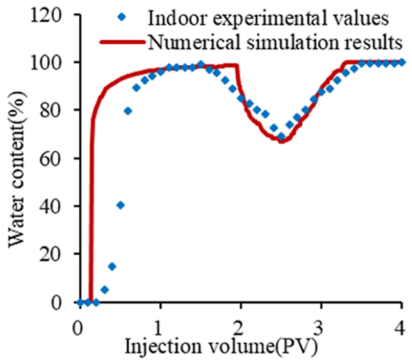

Figure 2. Variation in experimental and numerical model moisture content comparison.

numerical simulation is 62.56%, the experimental value is 63.69%, and the error rate is 1.81%. The validation results show that the established oil drive model of the soda-free ternary emulsion composite system can better simulate the actual situation.

2.2. Influence of Permeability on the Distribution of Components along the Path. A geological model is established, the number of grid is set to 54 × 54, the grid step length is 5 m, and a five-point well network is simulated with one injection and four extraction wells, where the injection and extraction wells are at the diagonal boundary of the model. The injection system is an alkali-free ternary emulsion composite system with an injection volume of 0.8 PV and an injection rate of 0.2 PV/a. The distribution of the alkali-free ternary emulsion composite system is simulated under different permeability conditions. From the simulation results, it can be seen that the chromatographic separation phenomenon also occurs during the oil-repelling process of the alkali-free ternary emulsification composite system.

By comparing the distribution along the system under different permeability conditions in Figures 3−5, it can be seen that the lower the permeability, the higher the separation of polymer, complex salt, and surfactant chromatography at the same injection volume. This is due to the fact that the lower the permeability, the larger the specific surface area of the rock pores, which in turn increases the adsorption of polymers and surfactants by the pores.

2.3. Influence of Injection Rate on the Distribution of Components along the Course. The model permeability is 300×10^{-3} μm^2, and the injection system is an alkali-free ternary emulsion composite system with a polymer concentration of 1800 mg/L and injection volume of 0.8 PV. The along-range distribution of the alkali-free ternary emulsion system is simulated under different injection rates (0.15, 0.2, 0.25 PV/a).

From the simulation results shown in Figures 6−8, it can be seen that the larger the injection velocity of the system, the less obvious the chromatographic separation of the soda-free ternary emulsion complex system, which is due to the increase of fluid velocity, which increases the driving force of the fluid on the soda-free ternary emulsion system and then decreases the adsorption of the polymer and complex salt by the rock pores and increases the transport and transportation capacity of the surfactant. However, the increase in injection velocity also intensifies the finger-in phenomenon of the system and reduces the system wave area.

https://doi.org/10.1021/acsomega.3c01433
ACS Omega 2023, 8, 40051−40062

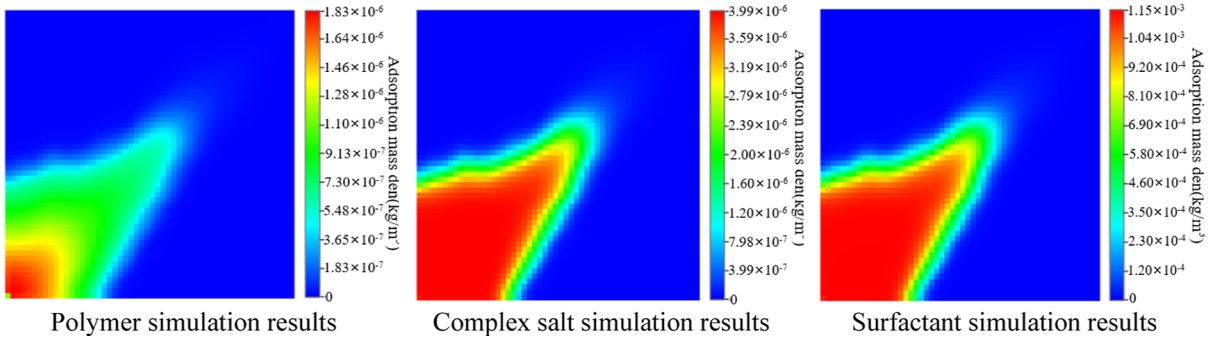

Figure 3. Simulation results of the distribution of the quality and efficiency improvement system along the range ($100 \times 10^{-3}\mu m^2$).

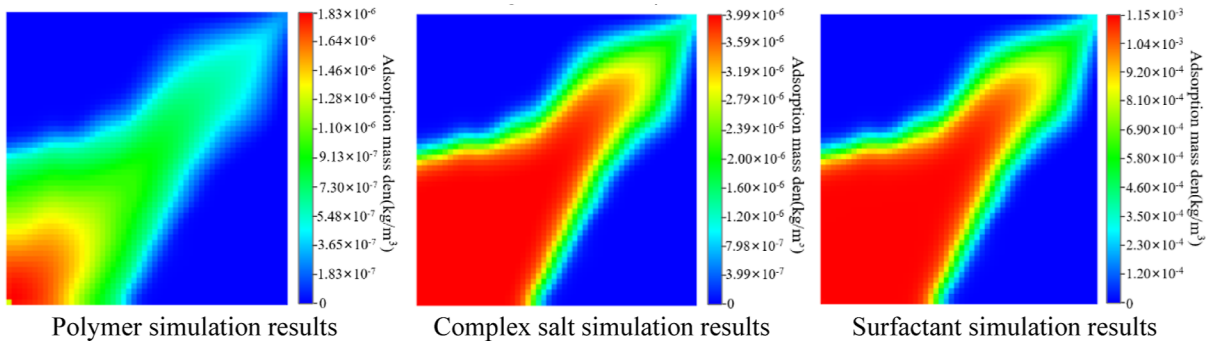

Figure 4. Simulation results of the distribution of the quality and efficiency improvement system along the range ($300 \times 10^{-3}\mu m^2$).

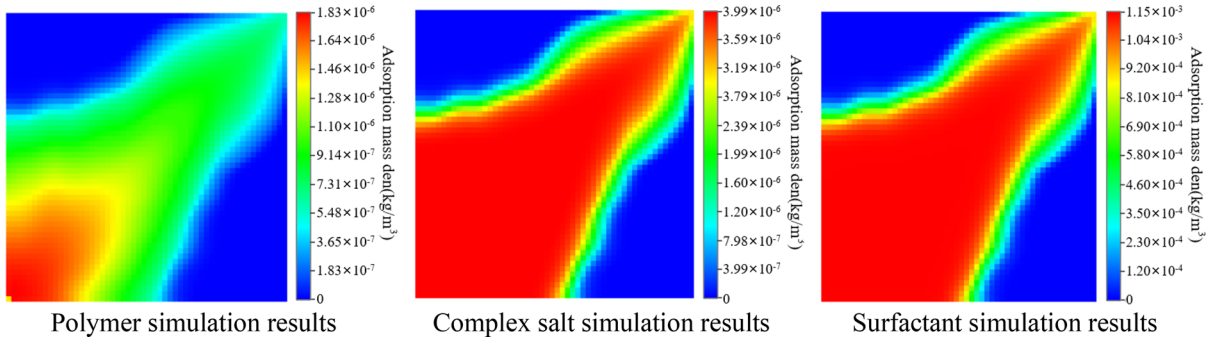

Figure 5. Simulation results of the distribution of the quality and efficiency improvement system along the range ($600 \times 10^{-3}\mu m^2$).

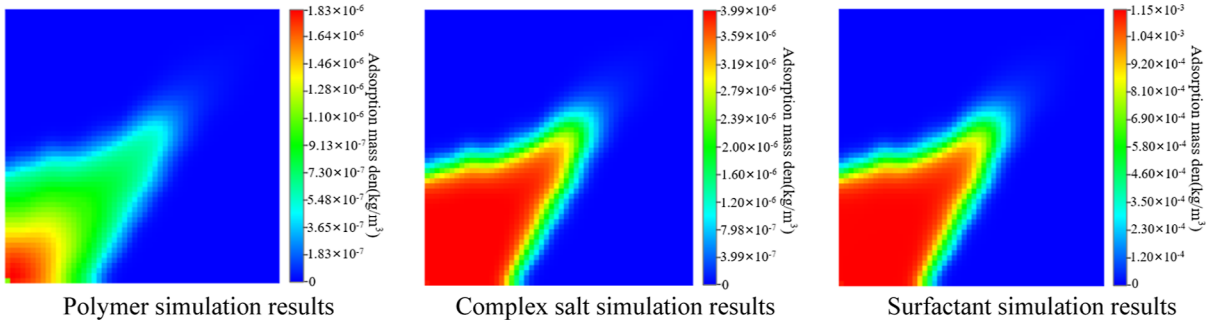

Figure 6. Simulation results of the distribution of the quality and efficiency improvement system along the range (0.15 PV/a).

2.4. Effect of Different Development Scenarios on Oil Recovery Effect. Simulate the production dynamics of different injection methods with a time step of 1 month and an injection rate of 0.2 PV/a. Scheme 1: water drive; Scheme 2: water drive to 98% water content followed by injection of alkali-free ternary emulsion system, compounded polymer injection concentration of 2200 mg/L, subsequent water drive to 98% water content; Scheme 3: water drive to 98% water content followed by injection of alkali-free ternary emulsion system, compounded polymer; Scheme 4: Multistage plug injection is selected; i.e., after water drive to water content, an alkali-free ternary emulsion system is injected with 0.5 PV, the polymer concentration in the compound is 2200 mg/L, the secondary plug is an alkali-free ternary emulsion compound

https://doi.org/10.1021/acsomega.3c01433
ACS Omega 2023, 8, 40051−40062

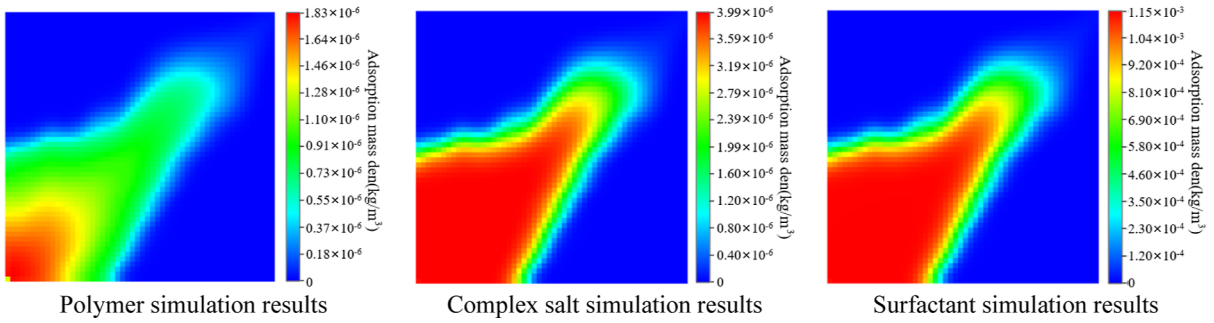

Figure 7. Simulation results of the distribution of the quality and efficiency improvement system along the range (0.2 PV/a).

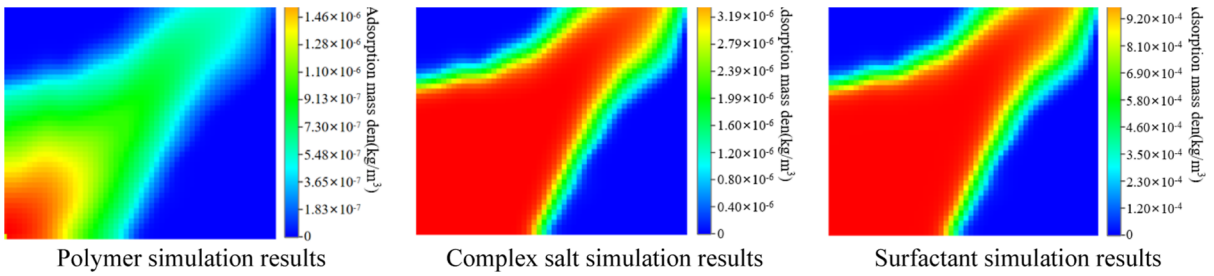

Figure 8. Simulation results of the distribution of the quality and efficiency improvement system along the range (0.25 PV/a).

system with 0.3 PV, the polymer concentration in the compound is 1800 mg/L, and the subsequent water drive to 98% water content.

When the polymer is injected, the recovery rate begins to significantly increase, and the injection pressure also increases accordingly. The variation pattern of the injection pressure is positively correlated with the injection concentration. In the subsequent water drive stage, due to the improvement of oil recovery, the formation pressure is lower than the pure water drive pressure. By comparing the dynamic change curves of recovery and water content of different injection schemes in Figures 9 and 10, it can be seen that the best recovery

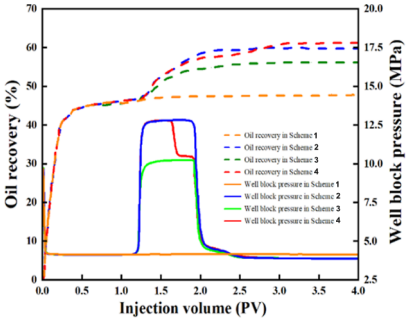

Figure 9. Dynamic curve of recovery rate and well block pressure with different injection methods.

enhancement effect is achieved by multistage plug injection. According to Figure 9, the water drive recovery rate and post polymer flooding recovery rate were obtained, and the effect of improving recovery rate was calculated and is summarized in Table 1. The total recovery rate of Scheme 4 is 61.59%, which is 16.06% higher than the recovery rate of water drive, and the recovery rate after the measure is 1.53 and 5.19% higher than that of Scheme 2 and Scheme 3, respectively.

In Scheme 4, the main section plug is injected with a high-concentration polymer and the subsection plug is injected with

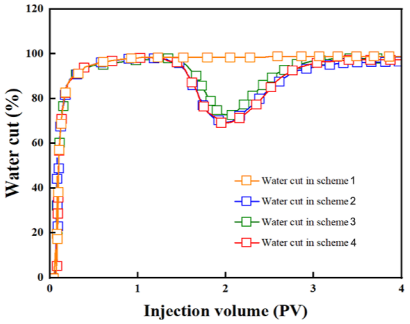

Figure 10. Dynamic curve of water content by different injection methods.

Table 1. Oil Drive Effect of Different Schemes

scheme	water drive recovery (%)	improved recovery after measures (%)	total recovery rate (%)
I	47.67		47.67
II	45.53	14.53	59.88
III	45.53	10.87	56.40
IV	45.53	16.06	61.59

a low-concentration polymer so that the high-viscous polymer enters the high permeability layer in priority and improves the resistance coefficient, which encourages the subsequent subsection plug solution to enter the low permeability layer and reduces the flow difference between the high permeability layer and the low permeability layer and brings into play the synergistic effect of compound salt and petroleum sulfonate surfactant to improve the reservoir activation and enhance the replacement effect.

3. CONCLUSIONS

In this article, a mathematical model of oil repelling with salt instead of alkali for the alkali-free ternary emulsification system is established, and the equation is discretized and solved in

https://doi.org/10.1021/acsomega.3c01433
ACS Omega 2023, 8, 40051−40062

terms of implicit pressure and explicit saturation. Numerical simulations and indoor physical experiments are carried out to verify the oil repelling effect of the alkali-free ternary emulsion system. By analyzing the distribution of permeability and injection rate along the system, the oil repelling effect of different development schemes is compared and the multistage plug injection method is preferred.

1 The alkali-free ternary emulsification system can exert the synergistic effect of compound salt and surfactant and maintain low interfacial tension and continuous emulsification phase during the whole process, which is conducive to the stripping and flooding of crude oil and can effectively improve the recovery rate.

2 The specific surface area of the pores of the low-permeability layer rocks is large, and the pores have a strong adsorption effect on the system, so the chromatographic separation of the alkali-free ternary emulsification composite system is high. Increasing the system injection speed and reducing the system wave area can reduce the degree of chromatographic separation in the alkali-free ternary emulsification composite system.

3 The results of indoor physical simulation and numerical simulation are verified with each other, and the difference between numerical simulation results and experimental values is small, and the error rate of recovery degree and total recovery rate of each stage is less than 2%. By analyzing the numerical simulation results of different development scenarios, the use of multistage plug injection can reduce the flow difference between high and low permeability layers and can effectively exert the synergistic effect of complex salt and surfactant to significantly improve the recovery rate, and the total recovery rate is 61.59%, which is 16.06% higher than the water drive recovery rate.

4. ANALYSIS METHOD

The material balance method is used to establish the transport equation of the soda-free ternary emulsion system, the materiality change equation in porous media is combined to construct a mathematical model for oil recovery of the soda-free ternary emulsion system considering a variety of influencing factors, and then the above equations are discretized by the finite difference method; the pressure and saturation are derived from the implicit pressure and explicit saturation and then solved.

In the process of establishing the derivative mathematical model, some assumptions are made to facilitate the solution, as follows: considering the existence of oil and water phases, the soda-free ternary emulsion system exists only in the water phase; both oil and water phases follow Darcy's law; the reservoir rock and oil−water are weakly compressible; considering the adsorption of the soda-free ternary emulsion system on the rock surface, the adsorption of the soda-free ternary emulsion system conforms to Langmuir isothermal adsorption; reservoir temperature remains stable.

4.1. Analysis of Influencing Factors. *4.1.1. Influence of Chemical Agent Concentration on the Change of Interfacial Tension.* In order to truly reflect the compound synergistic effect of multiple chemical agents, the measured interfacial tension isogram is used to describe that for a given crude oil and configuration water mineralization,[17] the interfacial tension mainly varies with surfactant, polymer, and emulsifier concentrations as follows.

$$\gamma = \gamma(C_{Na}, C_s, C_p, C) \tag{1}$$

4.1.2. Interfacial Tension Changes Due to Polymer Incorporation. The increase in interfacial tension between the alkali/surfactant/polymer system and the crude oil caused by the addition of a polymer is mainly considered.[18] Usually, the higher the polymer concentration, the more likely this phenomenon (which is a detrimental factor for oil drive) occurs. The following improvement can be made based on the experimental results: after the polymer concentration is greater than a certain value (∇C_{po}), the normally calculated interfacial tension (γ) of the AS system increases with the increase of the polymer concentration C_p, the magnitude of which is determined by the experimental data.

$$\nabla\gamma = f(\nabla C_{po}, C_p) \tag{2}$$

The addition of emulsifier makes the alkali-free ternary oil repellent system have similar ultralow interfacial tension interval and wider ultralow interfacial tension range.

4.1.3. Effect of the Emulsifier on the Oil-Repelling Effect. Emulsifier further broadens the activity range of surfactant and the pH range of spontaneous emulsification in alkali-free ternary system under high salt conditions by reducing the interfacial tension between oil and water. Under certain conditions, it forms a synergistic compensation effect with polymer, surfactant, and crude oil, improves the compatibility and solubilization of surfactant, and promotes the long-term stability of oil-containing emulsion during oil displacement Also, the industrial application process in the Daqing oilfield shows that the addition of an emulsifier can also reduce the adsorption of the polymer and surfactant in the formation, which reduces the injection amount of the alkali-free ternary system and reduces the damage to the reservoir.

4.1.4. Residual Saturation and Relative Permeability. The residual saturation of each phase is related to the number of capillaries, which is defined as follows.

$$N_c = \frac{|\sum_i \mu_i \vec{v}_i|}{\gamma} \tag{3}$$

$$S_{ri} = S_{ri}(N_c) \tag{4}$$

The residual saturation values at different N_c can be measured according to the experiment.[19] The relative permeability of each permeability group can be expressed as follows.

$$K_{ri} = K_{ri}^0 S_{ni}^{e_i} \tag{5}$$

$$S_{ni} = \frac{S_i - S_{ri}}{1 - \sum_i S_{ri}} \tag{6}$$

$$K_{ri}^0 = K_{ri}^0(N_c) \tag{7}$$

$$e_i = e_i(N_c) \tag{8}$$

where K_{ri}^0 and e_i are the relative permeability curve end point values and curve indices, respectively, which can be measured experimentally at different N_c.

4.1.5. Salt Consumption. Salt consumption is a very important factor in the composite drive of an alkali-free ternary emulsion system, which directly affects the success or

https://doi.org/10.1021/acsomega.3c01433
ACS Omega 2023, 8, 40051−40062

failure of an oil drive.[20] There are many factors affecting salt consumption, and it is complex; so this model will be processed with some simplifications to achieve the purpose of describing the main salt consumption phenomena better and having a strong practicality at the same time. The salt consumption in the model is described by the chemical reaction term R. It is expressed as follows.

$$R_{\mathrm{Na}}^{-} = -\phi S_{\mathrm{w}} \frac{\delta}{\delta t} \beta \frac{\alpha C}{1 + \alpha C} \tag{9}$$

where "−" is the consumption of Na^+; β is the salt consumption per unit volume; C is the concentration of Na^+; and α is the coefficient, determined from experimental data.

4.1.6. Surfactant Adsorption. The adsorption retention loss of surfactant can be described using the following equation

$$\Gamma_{\mathrm{s}}^{1} = \Gamma_{\mathrm{s}}^{0} \frac{a_{\mathrm{s}} C_{\mathrm{s}}}{1 + a_{\mathrm{s}} C_{\mathrm{s}}} \tag{10}$$

where Γ_{s}^{0} and a_{s} are related to the cation strength E, as determined from experimental information.

$$E = C^{+} + \delta C^{++} \tag{11}$$

where C^+ and C^{2+} are monovalent and divalent cation concentrations, mol/mL, respectively, and δ is a weighting factor. The adsorption retention of the surfactant will decrease with increasing pH in the formation water.

$$\Gamma_{\mathrm{s}} = \Gamma_{\mathrm{s}}^{1}\left(1 - b_{\mathrm{s}} \frac{\mathrm{pH} - 7}{\mathrm{pH}_{\max}}\right) \tag{12}$$

where Γ_{s}^{1} is the adsorption retention at pH = 7; $\mathrm{pH}_{\max}$ is the pH value of the formation water; and b_{s} is the coefficient.

4.1.7. Effect of Salt on Solution Viscosity. The addition of salt will cause changes in the salt environment of the solution, and the increase in the concentration of cations such as Na^+ will cause a significant decrease in the viscosity of the polymer solution, which is one of the most important adverse factors brought about by the addition of salt.[21]

$$\Delta\mu_{\mathrm{p}} = f(C^{+}, C^{++}) \tag{13}$$

4.1.8. Chemical Agent Diffusion Coefficient. The chemical agent diffusion coefficient is related to the flow rate.

$$\overline{U_{ri}} = \overline{U_{ri}^{0}} + \vec{v} U_{ii} \tag{14}$$

4.1.9. Capillary Pressure. For the case of the presence of the two phases of oil and water, capillary pressure is defined as $P_{\mathrm{c}} = P_{\mathrm{o}} - P_{\mathrm{w}}$. The capillary pressure of the composite system can be described as a function of oil−water capillary pressure and interfacial tension as follows.

$$P_{\mathrm{c}} = P_{\mathrm{cow}}(S_{\mathrm{w}}) \frac{\gamma}{\gamma_{\mathrm{ow}}} \tag{15}$$

$$P_{\mathrm{cow}}(S_{\mathrm{w}}) = C_{\mathrm{PN}} \sqrt{\frac{\phi}{K_{\mathrm{a}}}} (1 - S_{\mathrm{n}})^{M_{\mathrm{PN}}} \tag{16}$$

where C_{PN}, M_{PN}, and K_{a} are constants, determined by experimental research data, and S_{n} is the wet phase saturation.

4.1.10. Density of Each Phase of the Fluid. The density of each phase, ρ, depends on the pressure and composition of each phase and can be expressed as follows.

$$\rho = \rho_j^{0} \exp[\beta_j(\rho_j - \rho_j^{0})] \tag{17}$$

$$\rho_j = \frac{1}{\sum_i \frac{Y_i}{\rho_i^{0}}} \tag{18}$$

where ρ_j^0 and ρ_j are the reference pressure and the density at that pressure, respectively, and β_j is the compression coefficient.

4.1.11. Stationary Viscosity of the Polymer Solution. The resting viscosity (viscosity at zero shear rate) of a polymer solution is a function of the polymer solution concentration and salinity[22] and can be expressed as

$$\mu_{\mathrm{p}}^{0} = \mu_{\mathrm{w}}(1 + a_1 C_{\mathrm{p}} + a_2 C_{\mathrm{p}} + a_3 C_{\mathrm{p}} + \cdots) \tag{19}$$

where a_1, a_2, ... are empirical constants related to salinity, which can be determined by experimental data, and μ_{p}^0 is the resting viscosity of the polymer solution.

4.1.12. Kinematic Viscosity of Polymer Solutions in Porous Media. During the injection of a polymer in porous media, shear thinning of polymer leads to a decrease in the viscosity of polymer as the shear rate increases, which can be described by the Meter equation.[23]

$$\mu_{\mathrm{p}} = \mu_{\infty} + \frac{\mu_{\mathrm{p}}^{0} - \mu_{\infty}}{1 + \left[\frac{\nu}{\nu^{1/2}}\right]^{n-1}} \tag{20}$$

where μ_{p} is the kinematic viscosity of the polymer solution; μ_{p}^0 is the rest viscosity (viscosity at zero shear rate); μ_∞ is the viscosity at infinite shear rate (aqueous phase viscosity); ν is the shear rate; $\nu^{1/2}$ is the shear rate at $\frac{(\mu_{\mathrm{p}}^{0} + \mu_{\infty})}{2}$ viscosity; and nr is the power-law exponent of the non-Newtonian nature of the fluid, $1.0 < n < 1.8$. For Newtonian fluids, $n = 1.0$.

4.1.13. Polymer Adsorption. For static adsorption that approximately follows the Langmuir isothermal adsorption theory, the following equation is used for the calculation. The adsorption of polymers is considered to be reversible with respect to salinity and irreversible with respect to concentration.[24]

$$\Gamma_{\mathrm{p}} = \Gamma_{\mathrm{p}}^{\max} \frac{\beta_1 C_{\mathrm{p}}}{1 + \beta_2 C_{\mathrm{p}}} \tag{21}$$

where Γ_{p} is the maximum adsorption of the polymer on the rock surface at different salinities and β_1 and β_2 are the equilibrium adsorption constants, whose values can be determined in the laboratory.

For cases that do not conform to the Langmuir adsorption law, the adsorption amount can be calculated by interpolating the polymer adsorption curves at different salinity levels given by the laboratory.

4.1.14. Aqueous Phase Permeability Reduction Coefficient of Polymers. The decrease in water permeability caused by the adsorption hysteresis of the polymer can be described by the following equation.

$$R_{\mathrm{p}} = 1 + \frac{(R_{\max} - 1) q_{\mathrm{p}}}{q_{\mathrm{p}}^{\max}} \tag{22}$$

where q_{p} and R are the polymer adsorption retention and aqueous phase permeability decline factor under different salt contents and $q_{\mathrm{p}}^{\max}$ and $R^{\max}$ are the polymer saturation

https://doi.org/10.1021/acsomega.3c01433
ACS Omega 2023, 8, 40051−40062

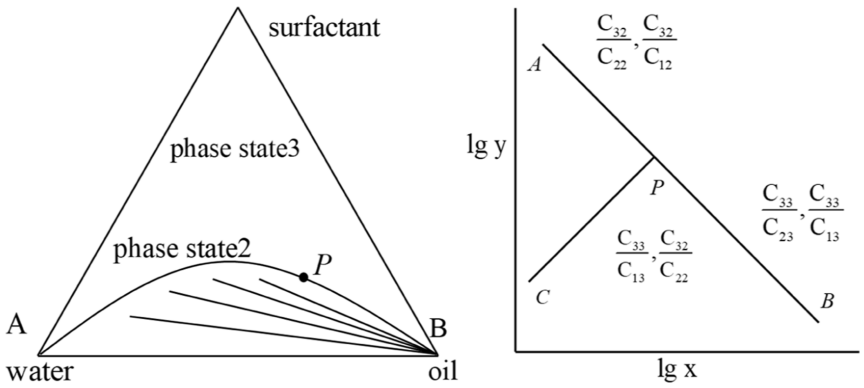

Figure 11. Triangular phase diagram and Hand diagram of the surfactant, water, and oil.

adsorption retention and maximum aqueous phase permeability decline factor under different salt contents.

4.1.15. Ion Exchange. The ionic exchange of monovalent cations in the aqueous phase with divalent cations on the rock surface increases the intensity of cations in solution ($C_{sep} = C^+ + \beta_c C^{++}$, weighting factor $\beta > 1$), which affects the viscosity and adsorption of the polymer, a phenomenon that can be described by the exchange equilibrium equation.

$$\frac{(C^+)^2}{C^{++}} = Q_v \beta_c \frac{(C^+)^2}{C^{++}} \tag{23}$$

$$C^+ + C^{++} = Q_v \tag{24}$$

where Q_v is the ion exchange capacity and β_c is the ion exchange coefficient.

4.1.16. Accessible Pore Volume of the Polymer.

$$\phi_p = \frac{V_p}{V} \tag{25}$$

where φ_p is the accessible pore volume of the polymer, which can be determined experimentally.

4.1.17. Characterization of Phase States of Oil-Repellent Systems. The phase theory of surfactant/oil/water considers the formation of three simulated components in solution from three volumetric components (oil, water, and surfactant).[25] The volume concentrations of these three components are usually combined into a triangular phase diagram. The salinity and divalent ion concentration strongly affect the phase state of the system. We already know that at low salinity, the excess oil phase is essentially pure oil, and the microemulsion phase includes water and electrolytes, surfactants, and some solvent oils, and this type of phase environment is known as Winsor type I or II(−). When the surfactant concentration is lower than the CMC value, the two phases contain all the surfactant, electrolyte, and a small amount of solvent oil liquid phase and pure oil-rich phase. For high salinity, there is an excess of water phase and a microemulsion phase containing most of the surfactant, crude oil, and partially dissolved water. This phase environment is called Winsor Type II or Type II (+), and the phase between II (−) and II (+) is called the third phase. These phases include the enriched oil phase, the excess water phase, and the microemulsion phase (whose composition is expressed by the fold points of the triangular phase diagram), and this phase environment is called Winsor type III or II. Other variables such as electrolyte concentration, alcohol type and concentration, equivalent alkane carbon number of the oil or solvent, and changes in pressure and temperature will cause a shift in the phase environment from one phase state to another, as shown by Yan et al.[26] Trichloroethylene (TCE) or chloride-based carbon mixtures and carbon tetrachloride have surfactant phase states that are identical to those of hydrocarbons; therefore, the relevant phase state methods for hydrocarbons can be used in these cases. The surfactant−oil−water phase state can be expressed as a function of the effective salinity when the double-nodal curve and the folded dotted line are plotted.

4.1.17.1. Optimal Salinity. If divalent ions are present, the optimum salinity decreases. For anionic surfactants, the optimum salinity increases when the temperature increases; for nonionic surfactants, the optimum salinity decreases when the temperature increases.

$$C_{se} = C^-(1 - af^s)^{-1}[1 + \beta_T(T - T_{ref})]^{-1} \tag{26}$$

where C^- is the anion concentration in the liquid phase; a is the normal number; f^s is the amount of divalent ions entering the surfactant micelles, $f^s = \frac{C_S}{C_3^m}$; and β_T is the temperature coefficient.

The optimal salinity at which triple equilibrium forms or disappears is called the upper or lower limit of optimal salinity (C_{sel} and C_{seu}).

4.1.17.2. Double Junction Curve Using Hand's Rule. The double junction curve equation can be changed to the same form for all phase environments, and Hand's rule is based on the experience that the phase equilibrium concentration ratio is a straight line in double logarithmic coordinates.[27] Figure 11 shows the type II triangle diagram with equilibrium phase and the corresponding Hand diagram. The double junction curve can be calculated by the following equation.

$$\frac{C_{3l}}{C_{2l}} = A\left[\frac{C_{3l}}{C_{2l}}\right]^B, \qquad l = 1,2,3 \tag{27}$$

where A and B are empirical parameters and for the symmetric double junction curve $B = -1$, the concentrations of all phases can be calculated based on the oil phase concentration $C_{2l}\sum_{k=1}^{3} C_{kl} = 1$ shown.

$$C_{3l} = \frac{1}{2}[-AC_{2l} + \sqrt{AC_{2l} + 4AC_{2l}(1 - C_{2l})}], \quad l = 1,2,3 \tag{28}$$

The parameter A is related to the height of the double-node curve as

https://doi.org/10.1021/acsomega.3c01433
ACS Omega 2023, 8, 40051−40062

$$A_m = \left[\frac{2C_{3\max,m}}{1 - C_{3\max+m}}\right]^m \qquad m = 0,1,2 \tag{29}$$

where m = 0,1,2 represent low salinity, optimum salinity, and high salinity, respectively, and the height of the double-node curve can be defined as a linear function of temperature as follows.

$$C_{3\max,m} = H_{BNC,m} + H_{BNT,m}(T - T_{ref}) \qquad m = 0,1,2 \tag{30}$$

where $H_{BNC,m}$ and $H_{BNT,m}$ are both input parameters and A_m is linearly interpolated as

$$A = (A_0 - A_1)\left[1 - \frac{C_{se}}{C_{seop}}\right] + A_1 C_{se} \le C_{seop} \tag{31}$$

$$A = (A_2 - A_1)\left[\frac{C_{se}}{C_{seop}} - 1\right] + A_1 C_{se} > C_{seop} \tag{32}$$

where C_{seop} is the optimum salinity, which is the arithmetic mean of C_{sel} and C_{seu}.

$$C_{seop} = \frac{1}{2}(C_{sel} + C_{seu}) \tag{33}$$

The principalities of the two-junction curves under the three parameters containing salinity are all input data, which can be obtained by estimating the fit based on the results of the phase experiment.

4.1.17.3. Two-Phase Fold-Point Line. For type II(−) and II(+) phase states, there are only two phase states under the double junction curve, and the connection line composed of equilibrium phases on the fold point line can be given by the following equation.

$$\frac{C_{3l}}{C_{2l}} = E\left(\frac{C_{33}}{C_{13}}\right)^F \tag{34}$$

where 1 = 1, 2 are type II(−) and type II(+) phase states, respectively. In the absence of fold point line data, $F = 1/B$; for the symmetric double junction curve $B = -1$, so $F = 1$. Therefore, the fold point is both on the double junction curve and on the fold point curve, so we have.

$$E = \frac{C_{1p}}{C_{2p}} = \frac{1 - C_{2p} - C_{3p}}{C_{2p}} \tag{35}$$

Substituting the double-node curve equation for the fold point and substituting C_{3p} into the above equation,

$$E = \frac{1 - C_{2p} - \frac{1}{2}[-AC_{2p} + \sqrt{AC_{2p}^2 + 4AC_{2p}(1 - C_{2p})}\,]}{C_{2p}} \tag{36}$$

where C_{2p} is the pleat point oil phase concentration and is the input value for both type II(−) and type II(+) phase environments.

4.1.17.4. Winsor III Type Phase Node Line. The phase composition of the Winsor III type three-phase region can be calculated by simply assuming that the excess oil and liquid phases are composed of a single line, and the microemulsion phase composition can be determined by the coordinates of the constant invariant point M. The point (M) is calculated from the optimum salinity as follows.[28]

$$C_{2M} = \frac{C_{se} - C_{csel}}{C_{seu} - C_{csel}} \tag{37}$$

Substitute C_{2M} into the formula to find C_{3M}.

$$C_{1M} = 1 - C_{2M} - C_{3M} \tag{38}$$

The calculation of the phase composition in the two-phase region from Winsor II(−) and Winsor II(+) is similar to the previous one, where the fold point needs to change from 0 to the Winsor II(+) value C_{2pr}* or from 0 to the Winsor II(−) value C_{2pr}*. Therefore, when considering only Winsor II(−), the fold point is calculated from the optimal salinity interpolation as

$$C_{2pr} = C_{2pr}^* + \frac{C_{se} - C_{sel}}{C_{seu} - C_{sel}}(1 - C_{2pr}^*) \tag{39}$$

In order to use the Hand equation, the concentration needs to be converted to the form shown in Figure 12, and the converted concentration is shown in the following equations.

$$C_{1l} = C_{1l}\cos\theta \tag{40}$$

$$C_{3l} = C_{3l} - C_{2l}\cos\theta C \tag{41}$$

$$C_{2l} = 1 - C_{1l} - C_{3l} \tag{42}$$

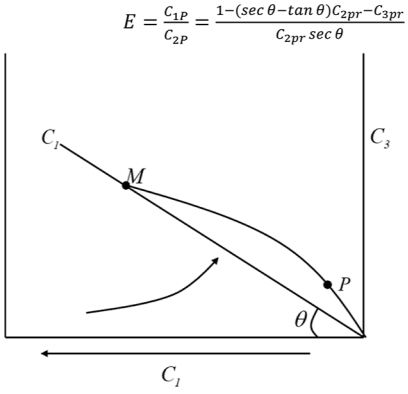

Figure 12. Calculated conversion coordinates of two phases in three phases.

The formula for calculating the inclination angle θ is shown in the following equations

$$\tan\theta = \frac{C_{3M}}{C_{1M}} \tag{43}$$

$$\sec\theta = \frac{\sqrt{C_{1M}^2 + C_{3M}^2}}{C_{1M}} \tag{44}$$

The parameter E of the node can be calculated from the fold point coordinate transformation as

$$E = \frac{C_{1P}}{C_{2P}} = \frac{1 - (\sec\theta - \tan\theta)C_{2pr} - C_{3pr}}{C_{2pr}\sec\theta} \tag{45}$$

In all subscripts p, s, Narepresent polymer, surfactant, salt, respectively; K is the absolute permeability, μm^2; k_{ro} and k_{rw} are the relative permeabilities of oil and water phases,

https://doi.org/10.1021/acsomega.3c01433
ACS Omega 2023, 8, 40051−40062

respectively;$\tilde{P}$o and $\tilde{P}$ware the oil and water phase pressures, MPa; S_o and S_w are the oil and water saturation, respectively; g is the acceleration of gravity, m/s^2; $h(x, y, z)$ is the depth, positive downward; c_Θ is the concentration of the corresponding repellant, $\Theta = \{p, s, \mathrm{OH}\}$ represents the polymer concentration, g/L, respectively; ρ_o, ρ_w, ρ_r are the densities of oil phase, water phase, and rock, kg/m^3, respectively; B_o and B_w are the volume coefficients of oil and water, respectively; μ_o, μ_w are the viscosities of oil and water phases after adding the repellant, mPa·s; R_k is the relative permeability decline coefficient; K_α is the parameter characterizing the magnitude of ion exchange and adsorption; K_{Na} is the adsorption constant of salt, cm^3/g; φ, φ_p, φ_s are the demonstrated porosity, polymer accessible porosity;$\phi_{p,s} = \phi f_{a,s}$, f_a, $f_s$are accessible porosity coefficients; ν_w is the percolation velocity, cm/s, inflow is positive; r_o and r_w are the flow coefficients of the oil and water phases, respectively,$\frac{\mu m^2}{mPa\cdot s}$; R_{Na} is the salt consumption, l/d; C_{rp} and C_{rs} are the mass of adsorbed polymer and surfactant per unit mass of rock, mg/g;$\tilde{q}_o$is the flow rate of the oil phase in the standard state, l/d, and the inflow is positive;$\tilde{q}_w$is the flow rate of the water phase in the standard state, l/d, and the inflow is positive;$\tilde{q}_c$, $\tilde{q}_d$, and$\tilde{q}_e$are the transport velocities of the wellbore repellant in g/(d L), l/(100 d), and l/(100 d), respectively;Di, i ∈ {w, o, OH}is the diffusion coefficient, m^2/s;Dij, i ∈ {w, o}, j ∈ {s, p} denotesthe diffusion coefficient of j in i, m^2/s; t is time,d; ∇ is Hamilton operator in the Cartesian coordinate system $\nabla = \frac{\delta}{\delta x}i + \frac{\delta}{\delta y}j + \frac{\delta}{\delta z}$; and x, y, z are the three directions of the Cartesian coordinate system and the unit of length is m.

In the model, both oil and water volume coefficients are a function of reservoir pressure $p(x, y, z, t)$, as follows.

$$B_o = \frac{B_{or}}{[1 + C_o(\tilde{P} - \tilde{P}_r)]} \tag{46}$$

$$B_w = \frac{B_{wr}}{[1 + C_w(\tilde{P} - \tilde{P}_r)]} \tag{47}$$

where$\tilde{P}$rdenotes the reference pressure (MPa), B_{wr} and B_{or} denote the water and oil volume coefficients at the reference pressure, respectively, and C_o and C_w denote the oil and water compression coefficients, respectively. The flow coefficient is calculated as shown in the following equation.

$$r_o = \frac{Kk_{ro}}{B_o\mu_o}, \; r_w = \frac{Kk_{rw}}{B_w R_k \mu_w} \tag{48}$$

The $f_w(x, y, z, t)$ is the water content as a function of the states$\tilde{P}$, S_w, c_s, and C_{OH}, which are defined as

$$f_w = \frac{r_w}{r_w + r_o} \tag{49}$$

The formula for calculating the surfactant concentration is shown below.

$$c_s = \frac{\tilde{q}_w c_{ws} + \tilde{q}_o c_{os}}{\tilde{q}_w + \tilde{q}_o} \tag{50}$$

4.2. Solution Equation Construction. In the process of establishing the derivative mathematical model, some assumptions are required to facilitate the solution, specifically the following assumptions: considering the effect of the soda-free ternary emulsion system on the phase change of oil and water fluids; both oil and water fluid flow follow Darcy's law; reservoir rocks and oil and water are weakly compressible; considering the adsorption of the soda-free ternary emulsion system on the rock surface, the adsorption of the soda-free ternary emulsion system conforms to Langmuir isothermal adsorption; and reservoir temperature remains stable.

4.2.1. Mass Conservation Equation. According to Darcy's law, the continuity of k-component mass can be expressed as the total volume of k-component in unit pore volume (k) as

$$\frac{\partial}{\partial t}(\phi \tilde{C}_k \rho_k) + \nabla[\sum_{l=1}^{n_p} \rho_k (C_{kl}\overline{U}_l - \tilde{D}_{kl})] = R_k \tag{51}$$

where the total pore volume of the component per unit pore volume includes the sum of all phases adsorbed.[29]

$$C_k = [1 - \sum_{k=1}^{n_{cv}} \tilde{C}_k]\sum_{l=1}^{n} S_l C_{kl} + \tilde{C}_k, \qquad k = 1,2, \ldots, n_c \tag{52}$$

where n_{cv} is the total number of components accounting for the volume; these components are water, oil, surfactant, and air bodies; n_p is the number of phases; $\tilde{C}_k$ is the adsorption concentration of k components; and ρ_k is the density of pure k components at the reference pressure p_R. The system can be assumed to be ideally mixed, with small variation and constant compressibility C_k^o; then, we have

$$\rho_k = 1 + C_k^o(p_R - p_{R_o}) \tag{53}$$

The amount of dispersion is assumed to be formed by Fick's law.

$$\tilde{D}_{kl,x} = \phi S_l K_{kl} \nabla C_{kl} \tag{54}$$

The dispersion expansion K_{kl} including molar diffusion (D_{kl}) can be calculated as follows.

$$\overline{K}_{kl,ij} = \frac{D_k}{\tau}\delta_{ij} + \frac{\alpha_{Tl}}{\phi S_l}[U]\delta_{ij} + \frac{\alpha_{Ll} - \alpha_{Tl}}{\phi S_l}\frac{U_{li}U_{lj}}{|\overline{U}_e|} \tag{55}$$

where α_{Ll} and α_{Tl} are the dispersions of phase l in the vertical and horizontal directions; τ is the curvature; U_{li} and U_{lj} are the Darcy flows of phase l in the i, j directions; δ_{ij} is the sign of the Kronecker Delta function; and the magnitude of the vector flow for each phase is

$$|\overline{U}| = \sqrt{(U_{xl})^2 + (\overline{U}_{yl})^2 + (\overline{U}_{zl})^2} \tag{56}$$

The phase flow rate of Darcy's law is

$$\overline{U}_l = -\frac{K_{rl}\overline{K}}{\mu_l}(\nabla p_l - \gamma_l \nabla h) \tag{57}$$

where $\overline{K}$ is the permeability tensor and h is the vertical depth. The source term R_k is the combination of all rate terms of a component and can be expressed as

$$R_k = \phi \sum_{l=1}^{n_p} S_i \gamma_{kl} + (1 - \phi)\gamma_{ks} + Q_k \tag{58}$$

where Q_k is the injection/output rate per unit volume of component k and γ_{kl} and γ_{ks} are the reaction rates of phase l and solid phase s.

4.2.2. Energy Conservation Equation. By assuming that energy is only a function of temperature and that energy in the

https://doi.org/10.1021/acsomega.3c01433
ACS Omega 2023, 8, 40051−40062

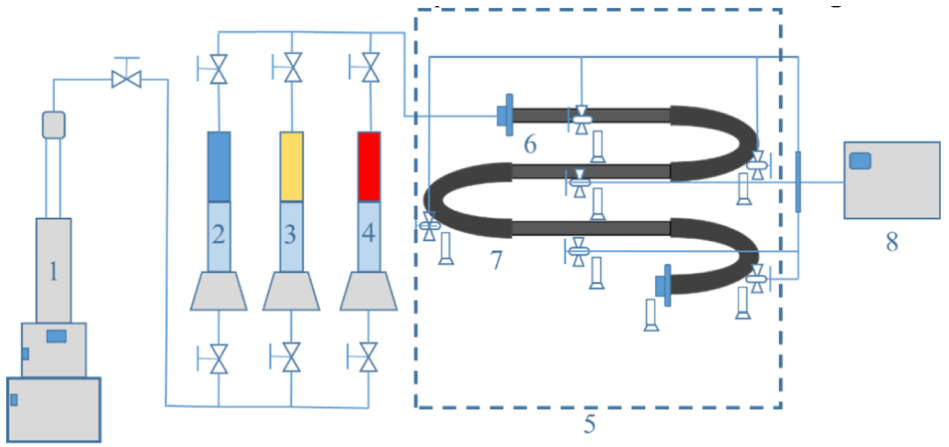

Figure 13. Schematic diagram of the experimental flow. (1) ISCO pump; (2) container for water formation; (3) container for crude oil; (4) container for alkali-free ternary emulsification system; (5) thermostats; (6) sampling points; (7) sand-filled pipe length core; and (8) pressure acquisition system.

oil or liquid phase proceeds only by convection and heat conduction, the energy balance equation can be derived as

$$\frac{\partial}{\partial t}[(1-\phi)\rho_s C_{vs} + \phi\sum_{l=1}^{n_p}\rho_l S_l C_{ve}]T + \nabla[\sum_{l=1}^{n_p}\rho_l C_{pl} U_l T - \lambda_T \nabla T] = q_H - Q_L \quad (59)$$

where T is the reservoir temperature; C_{vs} and C_{vl} are the heat capacities of solid and phase l at a constant volume; C_{pl} is the heat capacity of phase l at a constant pressure; λ_T is the heat transfer rate; q_H is the enthalpy source term per unit volume; and Q_L is the heat loss in the upper and lower covers and solid.

4.2.3. Pressure Equation. The capillary pressure is introduced by assuming the mass conservation equation for all components that account for the volume and replacing Darcy's law with the phase flow rate.

$$\sum_{k=1}^{n_{cv}} C_{kl} = 1 \quad (60)$$

The pressure equation can be derived as

$$\phi C_t \frac{\partial p_l}{\partial t} + \nabla \overline{K}\lambda_{rTc}\nabla p_l = -\nabla\sum_{l=1}^{n_p}\overline{K}\lambda_{rec}\nabla h + \nabla\sum_{l=1}^{n_p}\overline{K}\lambda_{rlc}\nabla p_{cl1} + \sum_{l=1}^{n_{cv}} Q_k \quad (61)$$

where $\lambda_{rec} = \frac{K_{rl}}{\mu_l}\sum_{k=1}^{n_{cv}}\rho_k C_{kl}$, $\lambda_{rTc} = \sum_{l=1}^{n_p}\lambda_{rec}$, λ_{rTc} is the total relative flow rate. The total compression coefficient C_t is the sum of the rock and solid compression coefficients.

$$C_t = C_r + \sum_{k=1}^{n_{cv}} C_k^o \tilde{C}_k \quad (62)$$

$$\phi = \phi_R[1 + C_r(p_R - p_{R_O})] \quad (63)$$

4.3. Model Validation. In order to check whether the established model can simulate the actual reservoir oil drive by an alkali-free ternary emulsion system, the results of indoor physical simulation experiments and numerical simulation results were validated against each other.

Two sets of 6 m long cores of sand-filled pipes were used for the indoor physical simulation, which consisted of different lengths of sand-filled pipes with diameters of 2.5 cm. The average permeabilities of the models were 497 and 504 mD, the pore volumes were 1154 and 1060 mL, and the porosities were 39.2 and 36.01%, respectively, at 50, 150, 250, 350, 450, 550, and 600 cm from the inlet position. Seven sampling points and pressure measurement points were set at 50, 150, 250, 350, 450, 550, and 600 cm from the inlet position. The whole experimental system consists of an ISCO metering pump, intermediate vessel, thermostat, long core experimental model, pressure acquisition system, etc. The experimental simulation uses formation water to saturate the core with a mineralization of 6778 mg/L, and the mineralization of the injected water is 5990 mg/L. The detailed experimental flow schematic and long core experimental model are shown in Figure 13.

The numerical simulation model simulates a five-point well network with one injection and four extraction wells in the center of the model and four extraction wells at the corners of the model. The injection system is the same as the indoor physical simulation experiment. The primary simulation is a water drive, and the simulation is stopped when the water content reaches 98%. The secondary simulation is an alkali-free ternary emulsion composite drive with an injection rate of 0.2 PV/a, and the simulation is stopped when the injection volume reaches 0.8 PV. The third simulation is a follow-up water drive phase with an injection rate of 0.2 PV/a, and the simulation is stopped when the water content reaches 98%.

AUTHOR INFORMATION

Corresponding Author

Jingchun Wu − *Key Laboratory of Enhanced Oil Recovery of Education Ministry, Northeast Petroleum University, Daqing 163318, China; College of Petroleum Engineering, Northeast Petroleum University, Daqing 163318, China;* Email: w6529@163.com

Authors

Xiaoying Liu − *Key Laboratory of Enhanced Oil Recovery of Education Ministry, Northeast Petroleum University, Daqing*

https://doi.org/10.1021/acsomega.3c01433
ACS Omega 2023, 8, 40051−40062

163318, China; First Oil Production Plant of Daqing Oilfield, Daqing Oilfield Co., Ltd, Daqing 163453, China

Jingang He − *First Oil Production Plant of Daqing Oilfield, Daqing Oilfield Co., Ltd, Daqing 163453, China*

Yinglong Xuan − *First Oil Production Plant of Daqing Oilfield, Daqing Oilfield Co., Ltd, Daqing 163453, China*

Hao Wu − *First Oil Production Plant of Daqing Oilfield, Daqing Oilfield Co., Ltd, Daqing 163453, China*

Sian Chen − *First Oil Production Plant of Daqing Oilfield, Daqing Oilfield Co., Ltd, Daqing 163453, China*

Yuan Yuan − *First Oil Production Plant of Daqing Oilfield, Daqing Oilfield Co., Ltd, Daqing 163453, China*

Haixiang Zhang − *College of Petroleum Engineering, Northeast Petroleum University, Daqing 163318, China; Sanya Offshore Oil and Gas Research Institute, Northeast Petroleum University, Sanya 572025, China*

Zhao Yang − *Key Laboratory of Enhanced Oil Recovery of Education Ministry, Northeast Petroleum University, Daqing 163318, China; College of Petroleum Engineering, Northeast Petroleum University, Daqing 163318, China;* orcid.org/0000-0003-0991-8689

Complete contact information is available at: https://pubs.acs.org/10.1021/acsomega.3c01433

Notes

The authors declare no competing financial interest.

■ ACKNOWLEDGMENTS

This work was supported by the General Project of National Natural Science Foundation of China of "Study on Mass Transfer Kinetics of Surfactants in Porous Media Under Electric Field" (51774088) and the General Project of Heilongjiang Natural Science Foundation of "Mechanism of biomethanation in tight oil reservoirs" (LH2022E020).

■ REFERENCES

(1) Pashapouryeganeh, F.; Zargar, G.; Kadkhodaie, A.; Rabiee, A.; Misaghi, A.; Zakariaei, S. J. S. Experimental evaluation of designed and synthesized Alkaline-Surfactant-polymer (ASP) for chemical flooding in carbonate reservoirs. *Fuel* **2022**, *321*, 124090.

(2) Chen, Z.; Han, X.; Kurnia, I.; Yu, J.; Zhang, G.; Li, L. Adoption of phase behavior tests and negative salinity gradient concept to optimize Daqing oilfield alkaline-surfactant-polymer flooding. *Fuel* **2018**, *232*, 71−80.

(3) Tan, X. J.; Zhang, J.; Wang, Y. N.; Li, M.; Liu, J.; Zhu, Z. Application of a Salt-Resistant In Situ Cross-Linked Terpolymer Gel for the Daqing Oilfield. *ACS Omega* **2023**, *8*, 22223−22229.

(4) Mehraban, M. F.; Farzaneh, S. A.; Sohrabi, M. Debunking the Impact of Salinity on Crude Oil/Water Interfacial Tension. *Energy Fuels* **2021**, *35*, 3766−3779.

(5) Wang, W.; Peng, Y.; Chen, Z.; Liu, H.; Fan, J.; Liu, Y. Synergistic Effects of Weak Alkaline-Surfactant-Polymer and SiO_2 Nanoparticles Flooding on Enhanced Heavy Oil Recovery. *Energy Fuels* **2022**, *36*, 7402−7413.

(6) Hamouma, M.; Delbos, A.; Dalmazzone, C.; Colin, A. Polymer Surfactant Interactions in Oil Enhanced Recovery Processes. *Energy Fuels* **2021**, *35*, 9312−9321.

(7) Zhao, J.; Torabi, F.; Yang, J. The role of emulsification and IFT reduction in recovering heavy oil during alkalinesurfactant-assisted CO_2 foam flooding: An experimental study. *Fuel* **2022**, *313*, 122942.

(8) Chung, J.; Holtsclaw, J.; Henderson, T. C.; Everett, T. A.; Schultheiss, N. C.; Boudouris, B. W.; Franses, E. I. Relationship of Various Interfacial Tensions of Surfactants/Brine/Oil Formulations to Oil Recovery Efficiency. *Energy Fuels* **2021**, *35*, 7768−7777.

(9) Tackie-Otoo, B. N.; Atta, D. Y.; Ayoub Mohammed, M. A.; Otchere, D. A. Investigation into the Oil Recovery Process Using an Organic Alkali-Amino Acid-Based Surfactant System. *Energy Fuels* **2021**, *35*, 11171−11192.

(10) Haghani Hassan Abadi, R.; Rahimian, M. H. Hybrid lattice Boltzmann finite difference model for simulation of phase change in a ternary fluid. *Int. J. Heat Mass Transfer* **2018**, *127*, 704−716.

(11) Nowrouzi, I.; Mohammadi, A. H.; Manshad, A. K. Chemical Enhanced Oil Recovery by Different Scenarios of Slug Injection into Carbonate/Sandstone Composite Oil Reservoirs Using an Anionic Surfactant Derived from *Rapeseed* Oil. *Energy Fuels* **2021**, *35*, 1248−1258.

(12) Li, Y.; Liu, H.; Wang, Q.; Dong, X.; Chen, X. Visual Filling Model Experiment Study on the Enhanced Oil Recovery Mechanism of Novel Polymer Viscosity Reducer Flooding in Heavy Oil Reservoirs. *ACS Omega* **2021**, *6*, 24663−24671.

(13) Sun, L.; Wu, X.; Zhou, W.; et al. Technologies of enhancing oil recovery by chemical flooding in Daqing Oilfield, NE China. *Pet. Explor. Dev.* **2018**, *45*, 673−684.

(14) Leuchtenberger, R. F.; Biazussi, J. L.; Verde, W. M.; Castro, M. d. S.; Bannwart, A. C. Experimental Analysis of Water/Oil Displacement Tests in Horizontal Pipe. *SPE J.* **2021**, *26*, 2993−3010.

(15) Corredor, L. M.; Ruiz-Cañas, M. C.; Rojas, J. A.; Llanos, S.; Castro-García, R. H.; Quintero, H. I.; Manrique, E.; Romero Bohórquez, A. R. Oil Displacement Efficiency of a Silica/HPAM Nanohybrid. *Energy Fuels* **2021**, *35*, 13077−13085.

(16) Liu, Q.; Wu, K.; Li, X.; Tu, B.; Zhao, W.; He, M.; Zhang, Q.; Xie, Y. Effect of Displacem ent Pressure on Oil-Water Relative Permeability for Extra-Low-Permeability Reservoirs. *ACS Omega* **2021**, *6*, 2749−2758.

(17) Abdulbari, H. A.; Amir, R. Drag Reduction Performance and Stability of an Organic Polymer, Surfactant, and Their Complexes. *Chem. Eng. Technol.* **2021**, *44*, 2333−2340.

(18) Xu, L.; Zhao, H.; Li, Y.; Cao, L.; Xie, X.; Zhang, X.; Li, Y. Production Optimization of Polymer Flooding Using Improved Monte Carlo Gradient Approximation Algorithm with Constraints. *J. Circuits Syst. Comput.* **2018**, *27*, 1850167.

(19) Zhai, Z.; Li, K.; Bao, X.; et al. Experimental studies on influence of temperature on relative permeability curves in sandstone reservoirs. *Energy Explor. Exploit.* **2022**, *40* (1), 206.

(20) Liu, Z.; Li, S.; Ge, Y. A quantum computing-based numerical method of mixed-integer optimal control problems under uncertainty for alkali-surfactant-polymer flooding. *Eng. Optim.* **2021**, *53*, 531−550.

(21) Ge, Y.; Li, S.; Chang, P. An approximate dynamic programming method for the optimal control of Alkai-Surfactant-Polymer flooding. *J. Process Control* **2018**, *64*, 15−26.

(22) Chen, S.; Han, M.; Alsofi, A. M. Synergistic Effects between Different Types of Surfactants and an Associating Polymer on Surfactant-Polymer Flooding under High-Temperature and High-Salinity Conditions. *Energy Fuels* **2021**, *35*, 14484−14498.

(23) Al-Anssari, S.; Ali, M.; Alajmi, M.; Akhondzadeh, H.; Khaksar Manshad, A.; Kalantariasl, A.; Iglauer, S.; Keshavarz, A. Synergistic Effect of Nanoparticles and Polymers on the Rheological Properties of Injection Fluids: Implications for Enhanced Oil Recovery. *Energy Fuels* **2021**, *35*, 6125−6135.

(24) Bridot, J. L.; Langevin, D.; Mullins, O. C. Role of Asphaltene Origin in Its Adsorption at Oil-Water Interfaces. *Energy Fuels* **2022**, *36*, 8749−8759.

(25) Kesarwani, H.; Saxena, A.; Saxena, N.; Sharma, S. Oil Mobilization Potential of a Novel Anionic Karanj Oil Surfactant: Interfacial, Wetting Characteristic, Adsorption, and Oil Recovery Studies. *Energy Fuels* **2021**, *35*, 10597−10610.

(26) Yan, W. H.; Yao, Z. J.; Shi, X. B.; et al. Experimental study on the displacement of oil by ASP weak alkali system in class III reservoirs. *Spec. Oil Gas Reservoirs* **2013**, *20*, 102−104.

(27) Li, S. R.; Ge, Y. L.; Zang, R. L. A Novel Interacting Multiple-Model Method and Its Application to Moisture Content Prediction of ASP Flooding. *Comput. Model. Eng. Sci.* **2018**, *114*, 95−116.

(28) Abdelfatah, E.; Wahid-Pedro, F.; Melnic, A.; Vandenberg, C.; Luscombe, A.; Berton, P.; Bryant, S. L. Microemulsion Formulations with Tunable Displacement Mechanisms for Heavy Oil Reservoirs. *SPE J.* **2020**, *25*, 2663−2677.
(29) Sigal, R. F.; Akkutlu, I. Y.; Kang, S. M.; et al. The Laboratory Measurement of the Gas-Storage Capacity of Organic Shales. *Petrophysics* **2013**, *54*, 224−235.

https://doi.org/10.1021/acsomega.3c01433
ACS Omega 2023, 8, 40051−40062